RESEARCH ARTICLE

Key Points:
- Multiple layers of anisotropy are present beneath Ethiopia
- Fossil, melt, and flow all generate anisotropy beneath Ethiopia
- Flow from the African superplume dominates flow in the sublithospheric mantle

Supporting Information:
- Read_Me
- Figures S1–S22
- Tables S1–S5

Correspondence to:
J. Hammond,
j.hammond@imperial.ac.uk

Differentiating flow, melt, or fossil seismic anisotropy beneath Ethiopia

J. O. S. Hammond[1], J.-M. Kendall[2], J. Wookey[2], G. W. Stuart[3], D. Keir[4], and A. Ayele[5]

[1]Department of Earth Science and Engineering, Imperial College London, London, UK, [2]Department of Earth Sciences, University of Bristol, Bristol, UK, [3]School of Earth and Environment, University of Leeds, Leeds, UK, [4]National Oceanography Centre Southampton, University of Southampton, Southampton, UK, [5]Institute of Geophysics Space Science and Astronomy, Addis Ababa University, Addis Ababa, Ethiopia

Abstract Ethiopia is a region where continental rifting gives way to oceanic spreading. Yet the role that pre-existing lithospheric structure, melt, mantle flow, or active upwellings may play in this process is debated. Measurements of seismic anisotropy are often used to attempt to understand the contribution that these mechanisms may play. In this study, we use new data in Afar, Ethiopia along with legacy data across Ethiopia, Djibouti, and Yemen to obtain estimates of mantle anisotropy using SKS-wave splitting. We show that two layers of anisotropy exist, and we directly invert for these. We show that fossil anisotropy with fast directions oriented northeast-southwest may be preserved in the lithosphere away from the rift. Beneath the Main Ethiopian Rift and parts of Afar, anisotropy due to shear segregated melt along sharp changes in lithospheric thickness dominates the shear-wave splitting signal in the mantle. Beneath Afar, away from regions with significant lithospheric topography, melt pockets associated with the crustal and uppermost mantle magma storage dominate the signal in localized regions. In general, little anisotropy is seen in the uppermost mantle beneath Afar suggesting melt retains no preferential alignment. These results show the important role melt plays in weakening the lithosphere and imply that as rifting evolves passive upwelling sustains extension. A dominant northeast-southwest anisotropic fast direction is observed in a deeper layer across all of Ethiopia. This suggests that a conduit like plume is lacking beneath Afar today, rather a broad flow from the southwest dominates flow in the upper mantle.

1. Introduction

Ethiopia is often cited as a natural laboratory for the study of the final stages of continental breakup [*Ebinger and Casey*, 2001; *Nyblade and Langston*, 2002; *Maguire et al.*, 2003]. However, debate still exists as to the mechanism that allows continents to break apart and for rifting to be sustained. The role that mantle upwellings [*Rogers*, 2006; *Chang and Van der Lee*, 2011], mantle flow [*Ebinger and Sleep*, 1998; *Hansen et al.*, 2012], melt [*Buck*, 2004; *Kendall et al.*, 2005; *Holtzman and Kendall*, 2010], and pre-existing lithospheric structure [*Vauchez et al.*, 2000; *Gashawbeza et al.*, 2004; *Cornwell et al.*, 2010] may play has been discussed widely, yet to date a consensus remains elusive. The study of seismic anisotropy, the variation of seismic wave speed with direction of propagation, offers the chance to differentiate between some of these mechanisms as it can highlight mantle flow through the alignment of olivine [*Babuska and Cara*, 1991], lithospheric fabrics [*Silver*, 1996], or the presence of aligned pockets of melt [*Kendall*, 2000]. A number of studies have attempted to unravel the anisotropic signature beneath Ethiopia [*Ayele et al.*, 2004; *Gashawbeza et al.*, 2004; *Kendall et al.*, 2005; *Sebai et al.*, 2006; *Montagner et al.*, 2007; *Sicilia et al.*, 2008; *Bastow et al.*, 2010; *Hammond et al.*, 2010; *Gao et al.*, 2010; *Obrebski et al.*, 2010; *Keir et al.*, 2011; *Hammond*, 2014], yet, to date, no consensus exists on the mechanisms causing the observed anisotropy. Here we use new data sets from Afar, Ethiopia combined with large data sets from Ethiopia, Yemen, and Djibouti to estimate shear-wave splitting beneath the Afar Triple Junction and surrounding regions. We use new, novel shear-wave splitting inversion techniques [*Wookey*, 2012] to unravel multiple layers of anisotropy beneath the rift, thus allowing us to place constraints on the dominant mechanisms of anisotropy beneath this complex tectonic setting.

2. Seismic Anisotropy

Mantle anisotropy is commonly associated with flow, which aligns the faster *a* axis of olivine crystals in the direction of flow (lattice preferred orientation, LPO) [*Babuska and Cara*, 1991]. However, other mechanisms

exist that also generate seismic anisotropy. These include the periodic layering of sediments or volcanics in the crust and the presence of preferentially oriented fractures, fabrics, or fluids in the crust and mantle (examples of shape preferred orientation, SPO). In volcanic settings, aligned melt either in the form of dikes and sills in the crust [*Hammond*, 2014] or oriented pockets of melt in the mantle [*Kendall et al.*, 2005] will cause seismic waves to travel faster parallel to the melt pockets than perpendicular to them. The amount of anisotropy depends on the aspect ratios and melt fractions, with even small amounts of melt generating considerable seismic anisotropy if the aspect ratios are low [see *Kendall*, 2000; *Holtzman and Kendall*, 2010, for review].

A common technique used to estimate anisotropy is shear-wave splitting [*Silver and Savage*, 1994]. As a shear wave enters an anisotropic medium, it will split into two orthogonally polarized quasi shear waves which travel at different speeds. This so called split shear wave allows us to characterize the symmetry of the anisotropic system (ϕ) and the time lag (δt) between the two shear waves can be used as a proxy for strength or thickness of the anisotropic medium. Commonly, core phases (*SKS*-waves and *SKKS*-waves) are used to investigate mantle anisotropy. These are shear waves which travel from the source as an *S*-wave, convert to a *P*-wave to travel through the outer core and convert back to an *S*-wave upon re-entering the mantle. The conversion to a *P*-wave, eliminates source side anisotropy. Typically, it is assumed that anisotropy is accrued in the uppermost mantle beneath the seismometer, as apart from the D″ layer at the core-mantle boundary, the rest of the mantle is largely isotropic [*Savage*, 1999]. Due to the near vertical ray path in the upper mantle, SKS-wave splitting gives very good lateral resolution beneath a station, but lacks depth resolution.

Silver and Savage [1994] show that in the presence of depth varying anisotropy, splitting parameters vary as a function of the initial source polarization of the shear wave. In the case of core phase splitting, the initial source polarization is the same as the back-azimuth (assuming no complexity at the core-mantle boundary). This variation has a characteristic $\pi/2$ variation, and thus allows for multiple layers of anisotropy to be identified, provided events from different back-azimuths are analyzed. Ethiopia meets this criteria being surrounded by subduction zone seismicity at the right distance (80°–140°), and having many stations deployed for long time periods (Figure 1). These data along with results based on other methods such as surface waves, which constrain azimuthal anisotropy (the variation of wave speed with the direction of propagation) and radial anisotropy (the variation of wave speed for vertically (Rayleigh) polarized and horizontally (Love) polarized waves) [*Sebai et al.*, 2006; *Montagner et al.*, 2007; *Sicilia et al.*, 2008; *Bastow et al.*, 2010], mean we can unravel the complex anisotropic signature seen beneath Ethiopia and place constraints on the driving forces behind rifting in East Africa.

3. Previous Studies of Anisotropy in East-Africa

Early studies of shear-wave splitting in East-Africa show anisotropic fast directions parallel to the Kenyan rift [*Gao et al.*, 1997; *Barruol and Hoffmann*, 1999; *Barruol and Ben Ismail*, 2001]. This suggested that olivine alignment due to passive upwelling, as expected for oceanic rifts [*Wolfe and Solomon*, 1998] was unlikely, as this would be oriented perpendicular to the rift. Rather, *Gao et al.* [1997] suggested that low upper mantle velocities [e.g., *Slack et al.*, 1994] indicated that hot material flowed along the rift, aligning olivine, a result consistent with more recent regional studies [*Bagley and Nyblade*, 2013]. More recently, *Gao et al.* [2010] investigated anisotropy in Ethiopia and proposed that the anisotropy is dominated in this region by flow in the asthenospheric mantle to the northeast, consistent with recent thermochemical convection models [*Forte et al.*, 2010; *Faccenna et al.*, 2013]. However, *Barruol and Ben Ismail* [2001] and *Gao et al.* [2010] show evidence for complicated splitting results as a function of back-azimuth in Kenya and Ethiopia/Djibouti, respectively, suggesting that more than one layer of anisotropy may be present.

Further evidence of multiple regions of anisotropy comes from studies using dense seismic networks in the Main Ethiopian Rift (MER). These show consistent fast directions trending rift parallel, but with time lags varying between ~1 and 3 s [*Gashawbeza et al.*, 2004; *Kendall et al.*, 2005]. These results show variations in splitting parameters above regions of Quaternary-recent volcanism, where a rotation in fast direction mimics the rotation in the Quaternary-recent volcanic segments. This was cited as evidence that oriented melt pockets dominate the anisotropy beneath the rift [*Kendall et al.*, 2005], but *Gashawbeza et al.*, [2004] argue that away from the rift pre-existing lithospheric structural fabrics play a role. Further evidence for a
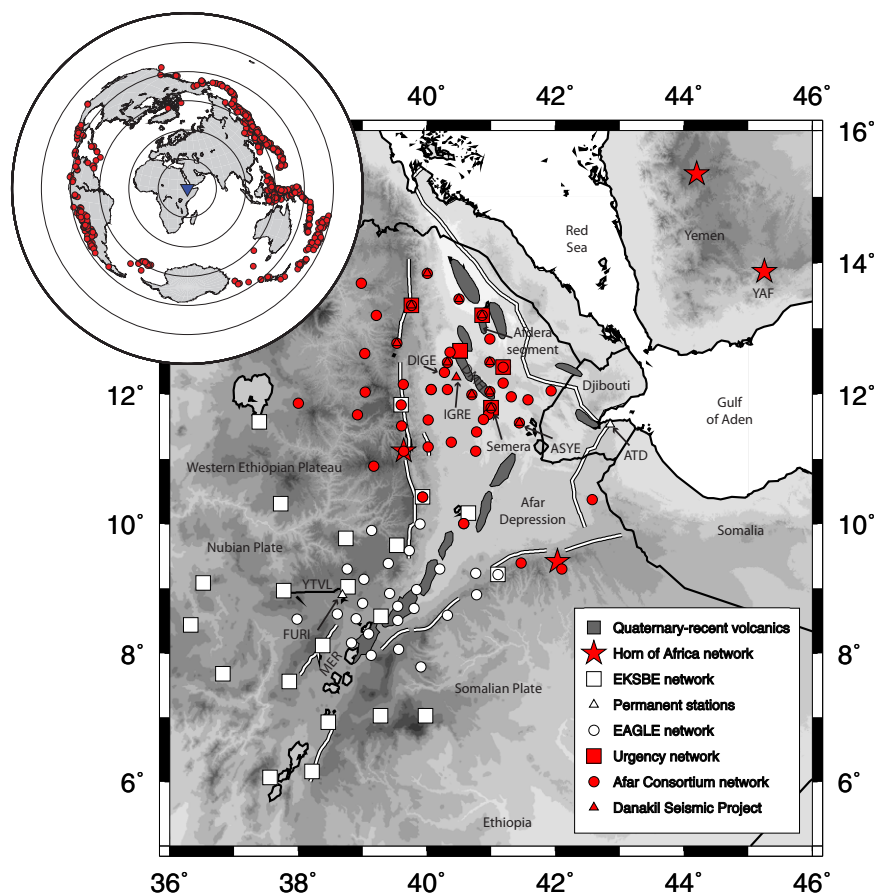
Figure 1. The seismic array, see legend for details of experiments. Stations in red show results not published previously. Stations in white show data that have been reanalyzed for this study. Thick white lines show major border faults and rift margins. Gray-filled regions show Quaternary-recent volcanic segments. The inset plot in the top left shows the earthquake distribution. Note the good back azimuthal coverage. YTVL: Yerer-Tullu Wellel volconotectonic lineament, MER: Main Ethiopian Rift, DMH: Dabbahu-Manda-Hararo segment. All other codes relate to seismic stations (see supporting information Table S1).

melt dominated anisotropic signal in the rift comes from *Ayele et al.* [2004] who show an increase in the amount of splitting in regions of increased volcanism. Also considerable crustal anisotropy is present, evidenced in studies of shear-wave splitting from local earthquakes [*Keir et al.*, 2005, 2011], and anisotropic receiver functions [*Hammond*, 2014]. These studies suggest that melt in the crust is a likely cause of anisotropy.

Surface waves offer another method to determine anisotropy beneath a region. They lack lateral resolution, but do offer depth constraints [*Montagner*, 1998]. Regional studies show a significant anisotropic signature in the uppermost mantle beneath East-Africa [*Sebai et al.*, 2006; *Montagner et al.*, 2007; *Sicilia et al.*, 2008; *Bastow et al.*, 2010]. *Sicilia et al.* [2008] invert for both radial and azimuthal anisotropy showing changes in anisotropic characteristics with depth. They argue that horizontal flow from a mantle plume beneath Afar is the cause of the deeper anisotropy, with possible fossil or melt-related anisotropy in the top 100 km [*Montagner et al.*, 2007; *Sicilia et al.*, 2008]. *Bastow et al.* [2010] compared radial and azimuthal anisotropy from surface waves and SKS splitting values showing that melt rather than channelized flow must be the cause of anisotropy in the uppermost mantle beneath the MER, which was further constrained to the top 90 km by waveform modeling of SKS phases [*Hammond et al.*, 2010].

The results of the previous work show that a significant anisotropic signature is present beneath East-Africa, but it is not clear what the dominant mechanism is. *Blackman et al.* [1993], *Kendall* [1994], *Blackman and Kendall* [1997], and *Wolfe and Silver* [1998] show that in a mid-ocean ridge setting anisotropy is likely a trade-off between LPO due to the passive upwelling of mantle material, and SPO due to aligned melt in the

lithosphere at the ridge axis. *Blackman and Kendall* [1997] show that at the ridge axis large amounts of aligned melt are expected resulting in large splitting. Away from the axis, where the amount of partial melt is likely insignificant, anisotropy is dominated by olivine alignment due to mantle flow, as is seen beneath the East-Pacific Rise [*Wolfe and Solomon*, 1998; *Harmon et al.*, 2004]. However, in a continental rift setting, the presence of old thicker lithosphere means that pre-existing structure can also produce significant aniso-tropy[*Silver*, 1996; *Vauchez et al.*, 2000] and any steep topography on the lithosphere-asthenosphere bound-ary will cause shear-derived segregation of melt to form bands of melt, another mechanism generating anisotropy [*Holtzman and Kendall*, 2010].

Beneath East Africa, multiple conduits of upwelling material have been proposed to exist [*Sebai et al.*, 2006; *Montagner et al.*, 2007; *Sicilia et al.*, 2008; *Chang and Van der Lee*, 2011], which would manifest itself as a radial [*Rümpker and Silver*, 2000] or circular [*Druken et al.*, 2013] pattern in azimuthal anisotropy. Alterna-tively, a more broad upwelling may be present, which flows along lithospheric topography, thus would flow toward the north-east beneath Ethiopia [e.g., *Ebinger and Sleep*, 1998; *Sleep et al.*, 2002; *Forte et al.*, 2010; *Hansen et al.*, 2012]. More recent studies imaging the upper mantle beneath Afar show that a conduit like plume is unlikely in the uppermost mantle beneath Ethiopia [*Rychert et al.*, 2012; *Hammond et al.*, 2013]. Rather decompression melting dominates at the rift axis [*Rychert et al.*, 2012], combined with small off-axis upper mantle diapiric upwellings [*Hammond et al.*, 2013]. These flow mechanisms potentially provide fur-ther localized anisotropic fabrics.

4. Data

Unraveling the expected complex anisotropic signals present in the splitting data requires data from a range of back azimuths. In our case, we are fortunate that over the last two decades many stations have been deployed throughout Ethiopia, and Ethiopia is also well located in terms of being surrounded by seis-micity at the right epicentral distance ($90°–140°$) (Figure 1). We use data from five temporary experiments, and two permanent stations deployed in Yemen, Ethiopia and Djibouti (Figure 1). New data come from nine stations deployed during the Afar urgency project [*Ebinger et al.*, 2008; *Keir et al.*, 2009] and a large NERC SEIS-UK [*Brisbourne*, 2012] and IRIS-PASSCAL deployment of 41 broadband seismometers which cov-ered most of the Afar Depression and surrounding highlands [*Belachew et al.*, 2011; *Hammond et al.*, 2011]. We include data in this study up until October 2010. Additionally, we provide new results from five French stations (RLBM (Réseau Large Bande Mobile)), deployed in Ethiopia and Yemen [*Sebai et al.*, 2006]. We also reanalyze data from the EKBSE (Ethiopia Kenya Broadband Seismic Experiment) [*Nyblade and Langston*, 2002] and the main deployment stage of EAGLE (Ethiopia Afar Geophysical Lithospheric Experiment) experi-ments [*Maguire et al.*, 2003]. We include two additional permanent stations; FURI, an IRIS run station in Ethiopia, and ATD, a GEOSCOPE run station in Djibouti. These permanent stations have been operational since 1993 (ATD) and 1997 (FURI). Many of the temporary deployments deployed stations in similar loca-tions (e.g., EKBSE, Afar Urgency, and Afar consortium all had stations in the Afar capital Semera, thus this location has 8 years of data and 149 SKS/SKKS splitting measurements) (see supporting information Table S1 and Figure S1).

5. Shear-Wave Splitting Measurements

We estimate splitting in *SKS/SKKS* phases using a semiautomated technique [*Teanby et al.*, 2004; *Wustefeld et al.*, 2010], based on the methodology of *Silver and Chan* [1991]. We filter the data between 3.3 and 20 s and rotate and time shift the horizontal components to find the combination of fast polarization angle and time delay which minimizes the second eigenvalue of the covariance matrix for particle motion for a time window around the phase. This linearizes the particle motion and usually results in minimizing energy on the transverse component (assuming the shear wave was radially polarized before entering the anisotropic medium). This gives us an estimate of the fast polarization direction (ϕ) and the time lag between the fast and slow shear waves (δt). We calculate 100 splitting measurements for 100 different windows and cluster analysis is used to identify the best result [*Teanby et al.*, 2004]. After a visual inspection of the good splitting data (looking for linearized particle motion, minimized transverse energy, and good signal-to-noise ratio), we further categorize the splitting results into good ($\phi_{error} < 10°$, $\delta t_{error} < 0.1s$), fair ($10° < \phi_{error} < 20°$, $0.1\,s < \delta t_{error} < 0.2s$) and poor (($20° < \phi_{error} < 30°$, $0.2s < \delta t_{error} < 0.3s$)) results. We only categorize the
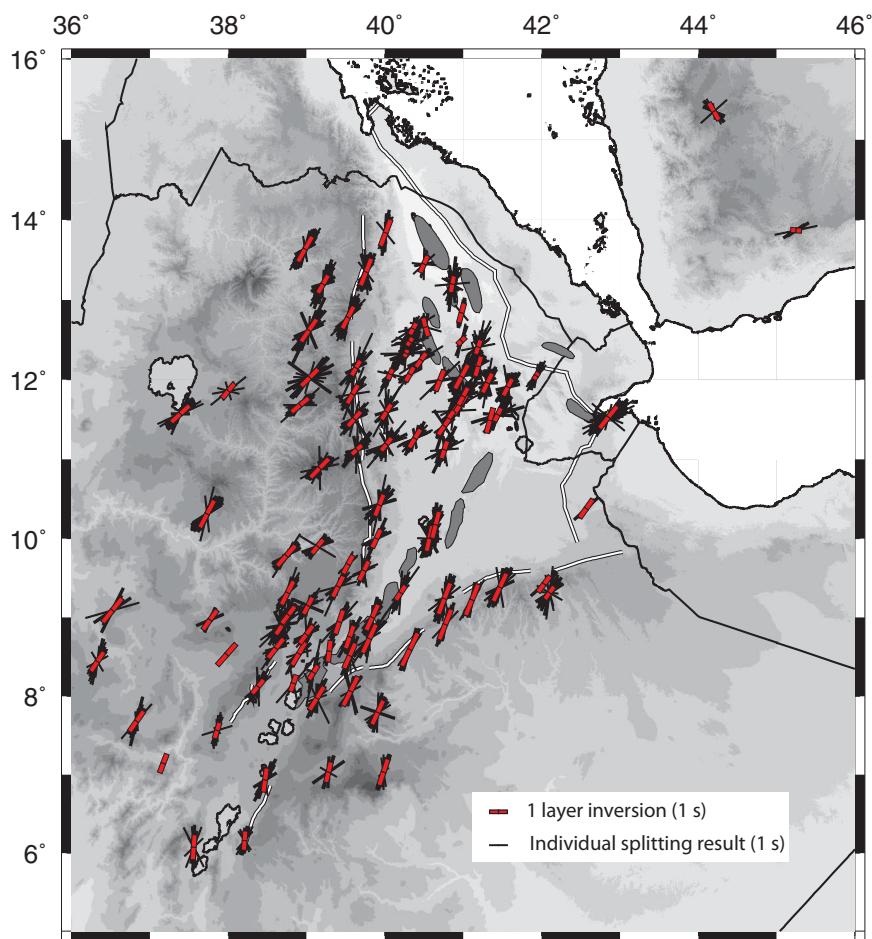
Figure 2. Individual and one-layer inversion splitting results. Thin black lines show the individual good and fair splitting results (see text for definition). Red lines show the one-layer inversion result for all stations.

data for plotting purposes, all data are used in the multiple layer shear-wave splitting inversions as even poorly constrained results can add useful constraints in the inversion. In some cases, no splitting is seen in the incoming shear waves, even when signal is clear. These so called null events can either be due to the initial polarization of the shear wave being similar to the symmetry axis of the anisotropy or the structure beneath the station is isotropic [*Wustefeld and Bokelmann*, 2007]. These data are included in the multiple layer shear-wave splitting inversions as they add valuable constraints. In total, we use 691 earthquakes (supporting information Table S2) estimating shear-wave splitting in 3092 phases (supporting information Table S3) and identify a further 845 null results (supporting information Table S4). An example splitting result and null result is shown in supporting information Figure S1 and good, fair, and stacked results are shown in Figure 2.

Similar to previous studies of shear-wave splitting in Ethiopia [*Ayele et al.*, 2004; *Gashawbeza et al.*, 2004; *Kendall et al.*, 2005; *Gao et al.*, 2010], we observe a dominant northeast-southwest fast direction across the whole data set, with the suggestion of more north-south fast directions toward the northernmost Afar/Plateau region and more east-west orientations close to the southeastern plateau (Figure 2). The only exceptions are three urgency stations (treated as one station in this study as they are almost colocated) deployed above the region of recent diking activity on the Dabbahu-Manda-Hararo volcanic segment which show fast directions in a north-south orientation, parallel to the dike orientation (Figure 2).

Interestingly, some of the seismic stations show considerable variation in splitting parameters with back-azimuth (Figure 3). *Gao et al.* [2010] showed that station ATD has a 2π variation with back-azimuth,
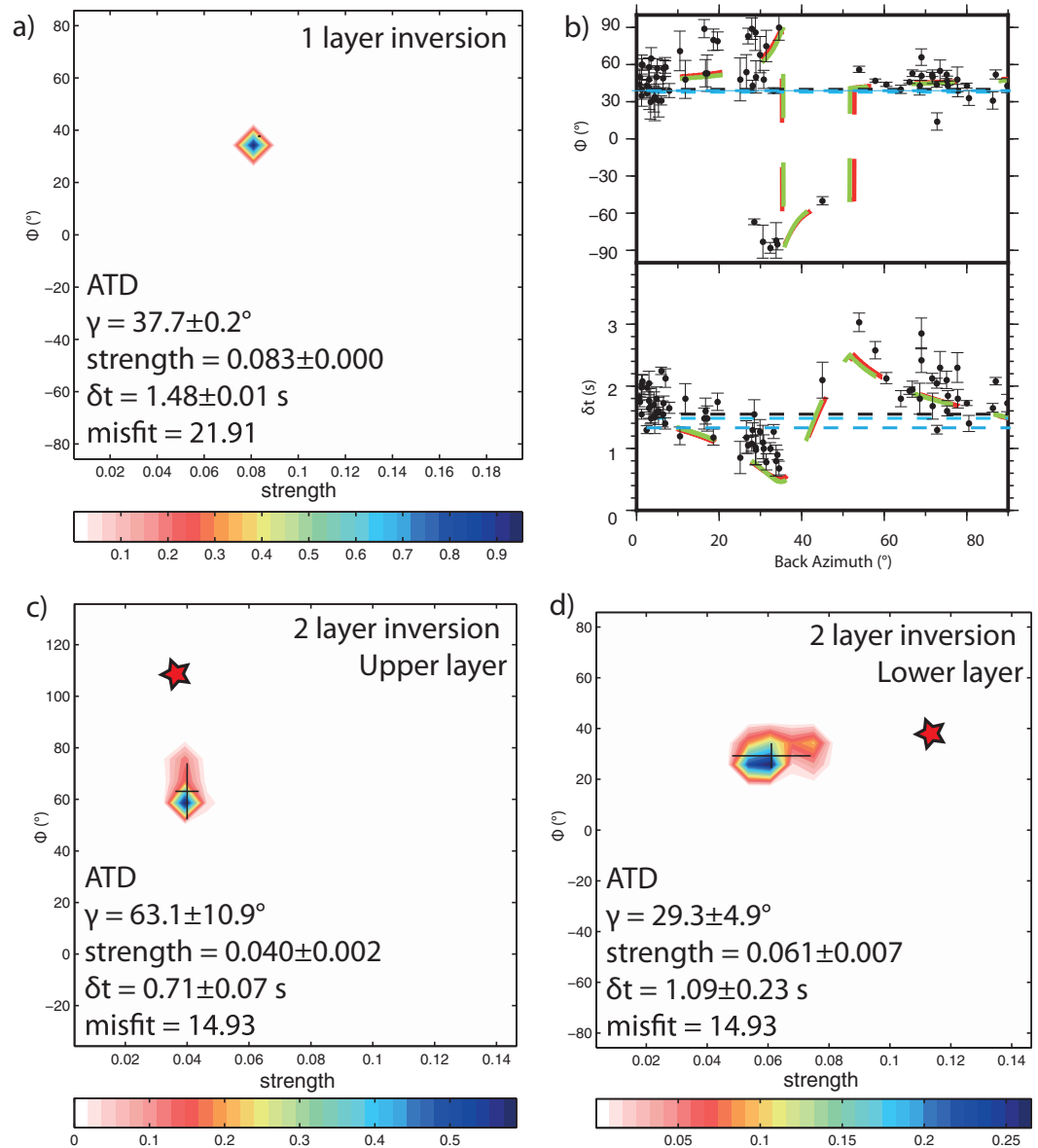
Figure 3. Example shear-wave splitting inversions for station ATD. (a) The one-layer splitting inversion. (b) Theoretical two-layer shear-wave splitting curves [*Silver and Savage*, 1994] for the error surface stacking [*Restivo and Helffrich*, 1999] (dashed black line), the one-layer inversion (dashed blue line), the two-layer inversion (red), and the two-layer result of *Gao et al.* [2010] (green). Note the similarity between the green and red curves. The two-layer inversion result for (c) the upper layer and (d) the lower layer. The red star shows the two-layer result of *Gao et al.* [2010] ($\phi_{upper} = -71°$, $\delta t_{upper} = 0.65s$, strength $_{upper} = 0.037$, $\phi_{lower} = 38°$, $\delta t_{lower} = 2.00s$, strength $_{lower} = 0.113$).

indicative of multiple layers of anisotropy [*Silver and Savage*, 1994]. *Obrebski et al.* [2010] used surface waves and P-wave receiver functions at ATD showing that multiple layers of anisotropy are consistent with these seismic data sets. With our new data, we show that many other stations throughout Afar also show the signature of multiple layer anisotropy with systematic variation in fast direction and time lag with back-azimuth (Figure 3 and supporting information Figures S1–S21).

6. Multiple Layer Shear-Wave Splitting Inversions

Previous studies investigating multiple layers of anisotropy [*Barruol and Hoffmann*, 1999; *Barruol and Ben Ismail*, 2001; *Gao et al.*, 2010] have attempted to model them using the theoretical curves of *Silver and Savage* [1994]. This works well as a method of hypothesis testing, however, there remains an inherent

ambiguity in inverting data using this technique as differing parameters for two layer splitting can have very similar curves [*Wookey*, 2012]. For example, the best fitting two layer case for station ATD suggested by *Gao et al.* [2010] (upper layer: −71°, 0.65 s, lower layer: 38°, 2.0 s) has almost identical theoretical curves to that shown for a case with markedly different splitting parameters (upper layer: 63°, 0.71 s, lower layer: 29°, 1.09 s) (Figure 3).

Here we use a newly developed shear-wave splitting inversion method [*Wookey*, 2012]. This technique allows us to split the region beneath a seismic station into box-shaped domains. Within each domain, it is assumed that a constant anisotropy exists, given an 81 component fourth rank tensor (**C**), which can be represented by a 6 × 6 matrix without loss of information (Voight notation). Two parameters are varied in each domain. The angle of anisotropic symmetry (−90°–90°) (assuming a HTI medium) and the strength parameter (0–0.15) (a factor which determines the dilution of **C** by Voight-Reuss-Hill averaging). A strength factor of 0.1 equates to ∼1.7 s of splitting assuming a 40 km thick layer. We place no constraints on the thickness of the layer due to the trade-off of strength with layer thickness, for example a 0.05 strength over an 80 km thick layer will give the same results as that for a 0.1 strength and 40 km thick layer. By systematically rotating and diluting the base elastic constants, we can calculate the anisotropic tensor for a suite of symmetry axes and strength factors. From this it is possible to calculate the polarization and phase velocity of the two shear waves (thus the expected ϕ and δt) by solving the Christoffel equation. With this information, we can define the shear-wave splitting operator for each domain in our model (Γ_i, defined by ϕ and δt in the domain). We then correct the real data for these modeled splitting operators and measure the second eigenvalue of the particle motion (λ_2) after correction. This is the key step in the *Wookey* [2012] shear-wave splitting technique as it allows us to minimize the summed λ_2 for all waveforms in the data set. The *Silver and Chan* [1991] technique estimates shear-wave splitting parameters by minimizing λ_2, thus the *Wookey* [2012] shear-wave splitting technique incorporates the analysis step of the data into the inversion mechanism itself thus removing any need to deal with complex misfit functions inherent in comparing the modeled and measured fast polarization and time lags [see *Wookey*, 2012, for more details]. This step also allows us to include null data into the inversion with no special treatment. To evaluate each candidate model, we calculate a reduced chi-square misfit

$$\chi^2 = \frac{1}{\nu} \sum_{i=1}^{N} \frac{\lambda_{2,i}}{\sigma_{\lambda,i}}$$

where ν is the number of degrees of freedom (taken to be the number of seismograms inverted minus the free parameters in the model), $\lambda_{2,i}$ is the normalized second eigenvalue of the *i*th seismogram, and $\sigma_{\lambda,i}$ is its associated error, estimated from an initial standard splitting analysis of the data. In all, one and two layer models tested the misfit is significantly larger than one. This implies that the modeling is not spuriously fitting noise, but that also there is still complexity in the data which the model is not capturing. Improvements in misfit reduction do, therefore, imply a better fitting model.

Figure 3 shows an example inversion for station ATD. We show that the crust and mantle beneath ATD is best fit (misfit = 14.93) by two layers of anisotropy with a fast orientation of 63 ± 11°, and delay time of 0.7 ± 0.1 s in the upper layer and a fast orientation of 29 ± 5° and delay time of 1.1 ± 0.2 s in the lower layer. The results have a lower misfit than the model shown by *Gao et al.* [2010] (misfit = 16.61) which has a fast orientation of −71° and delay time of 0.65 s in the upper layer and fast orientation of 38° and delay time of 2.0 s in the lower layer.

The first step to systematically constrain anisotropy beneath Ethiopia is to determine how well a single layer of anisotropy can match the data. We construct a model with one domain for each seismic station and invert the data. We compare this with the error surface stacking technique of *Restivo and Helffrich* [1999] (supporting information Table S5 and Figure 3). It is clear that both techniques give similar results.

To invert more than one layer of anisotropy, we follow the workflow shown in Figure 4. It is important that we have good back-azimuthal coverage [*Wookey*, 2012]. We set a criteria that a station must have at least eight splitting measurements across five different 10° bins (supporting information Table S5). All stations that pass this test are then inverted for a two-layer model. To identify stations which show robust two-layer splitting characteristics, we apply the following tests:
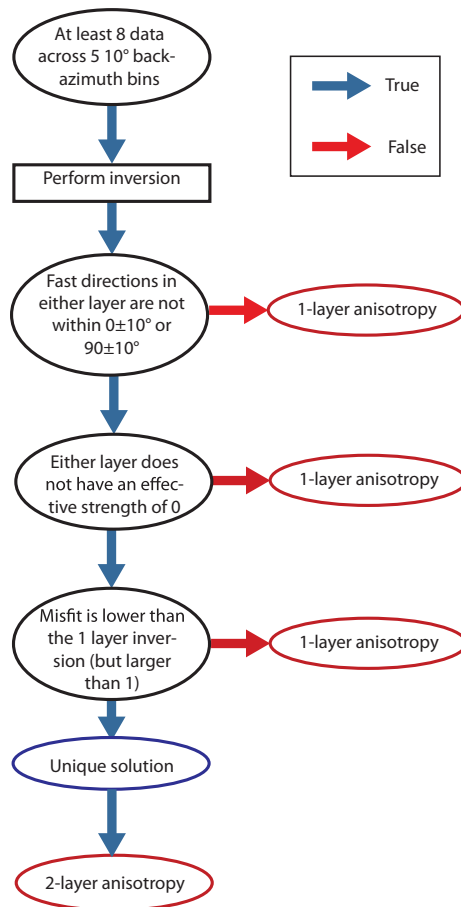
Figure 4. The workflow followed in performing the two-layer inversions.

1. The two-layer inversion has fast directions which are not within $0 \pm 10°$ or $90 \pm 10°$ of each other (i.e., close to the same fast direction, or orthogonal fast directions).

2. None of the layers in the two-layer inversion have an effective strength, accounting for errors, of 0.

3. The misfit for a two-layer inversion must be lower than that for a one-layer inversion.

4. The two-layer inversion must show a unique solution.

In total, 22 stations passed this test, while 67 stations are either best fit with one layer of anisotropy, orthogonal layers of anisotropy or have no unique solution. Fourteen stations do not have enough data from enough back-azimuths for us to invert. Figure 3 shows the two-layer inversions for station ATD (all other results are shown in supporting information Figures S2–S21) and Table 1 and Figure 5 show the best fitting two-layer results.

7. Results

7.1. Ethiopian Plateau and Yemen
Evidence for two layers of anisotropy in the Ethiopian plateau and Yemen are sparse. One station, YAYE in Ethiopia, shows some evidence for upper layer anisotropy, but foliation direction beneath this station is unclear. Station YAF in Yemen shows upper layer orientations which match major geological features [*Windley et al.*, 1996]. The lower layer beneath the Ethiopian plateau is oriented northeast-southwest and beneath Yemen mimics the orientation of the Red Sea and Gulf of Aden rifts (Figure 5).

7.2. Main Ethiopian Rift (MER)
The upper layer beneath the MER has fast directions aligned rift parallel, except for two distinct east-west fast directions which lie close to the east-west trending chain of volcanoes called the Yerer-Tullu Wellel volconotectonic lineament (YTVL) (Figure 5). The lower layer beneath the MER has consistent northeast-southwest oriented fast directions (Figure 5).

7.3. Afar Depression
Beneath the Afar Depression a complicated pattern of two-layer anisotropy is observed. Close to the large border faults at the western margin of the Afar Depression, a strong two-layer anisotropy signature is observed (Figure 5). The fast directions in the upper layer align parallel to the border faults (e.g., HALE, ABAE, BTIE, and SHEE), with a significant strength present (<0.13 or <2.25 s). Other stations in Afar, which lie close to the present day rift axis, expressed at the surface by segments of Quaternary-recent volcanism, show fast directions which parallel these segments (e.g., ATD and GEWE), and mimic the trends seen in the upper mantle S-wave velocity structure (Figure 6). There exists one more region of anomalous upper layer anisotropy beneath Afar. Three stations (DIGE, IGRE, and HARE) (Figure 1) show fast directions with an east-west orientation (Figure 5). The lower layer beneath the Afar Depression shows a consistent northeast-southwest orientation, although two stations (ASYE and DIGE) (Figure 1) do show more northwest-southeast and north-south orientations (Figure 5).

While there exist 22 stations with clear examples of two layers of anisotropy, 67 show that one layer best fits the results. This implies that either just one layer of anisotropy is present, or if more than one layer exists

Table 1. Two-Layer Inversion Results.

Station	Latitude (°)	Longitude (°)	One-Layer Misfit	Two-Layer Inversion				Misfit
				Upper Layer		Lower Layer		
				ϕ (°)	Δt (s)	ϕ (°)	Δt (s)	
AAUS	9.03	38.77	39.77	23.6 ± 5.1	1.11 ± 0.07	71.7 ± 3.2	0.56 ± 0.06	32.62
ABAE	13.35	39.76	23.70	16.2 ± 4.0	1.24 ± 0.16	60.7 ± 7.1	0.37 ± 0.06	19.88
ADTE	11.12	40.76	22.27	34.0 ± 4.5	0.34 ± 0.06	12.2 ± 5.6	0.69 ± 0.06	21.80
ADUE	8.54	38.90	45.83	100.3 ± 14.8	0.60 ± 0.30	29.8 ± 5.7	1.98 ± 0.31	34.94
AMME	8.30	39.09	11.47	193.9 ± 4.1	0.95 ± 0.07	71.8 ± 4.1	0.60 ± 0.06	9.09
ASYE	11.56	41.44	34.83	36.1 ± 5.1	1.43 ± 0.31	−42.4 ± 4.5	0.86 ± 0.33	22.97
ATD	11.53	42.85	21.91	63.1 ± 10.9	0.71 ± 0.07	29.3 ± 4.9	1.09 ± 0.23	14.93
BELA	6.93	38.47	81.43	75.1 ± 14.4	0.90 ± 0.47	7.1 ± 7.9	1.95 ± 0.50	78.92
BTIE	11.19	40.02	42.98	−30.8 ± 10.1	0.95 ± 0.48	46.3 ± 6.1	1.65 ± 0.60	36.16
BUTE	8.12	38.38	88.19	−4.3 ± 3.5	0.70 ± 0.07	50.5 ± 4.4	1.21 ± 0.06	69.17
CHAE	9.31	38.76	16.91	42.6 ± 5.6	0.86 ± 0.43	13.0 ± 18.0	0.65 ± 0.25	13.76
DIGE	12.33	40.27	101.24	67.5 ± 6.6	1.09 ± 0.28	−8.2 ± 4.7	1.48 ± 0.34	80.38
DONE	8.51	39.55	11.58	15.3 ± 5.7	1.62 ± 0.08	74.2 ± 3.8	0.43 ± 0.06	8.75
GEWE	10.00	40.57	30.24	33.7 ± 19.7	0.48 ± 0.23	4.2 ± 4.8	1.01 ± 0.34	28.54
GTFE	9.00	39.84	10.58	19.4 ± 4.6	1.35 ± 0.07	62.7 ± 4.3	0.16 ± 0.06	10.51
HALE	13.84	40.01	12.53	16.1 ± 6.3	2.25 ± 0.59	95.8 ± 9.1	0.95 ± 0.53	10.51
HARE	11.61	40.88	28.64	86.0 ± 21.4	0.58 ± 0.06	27.6 ± 6.9	1.00 ± 0.33	22.90
IGRE	12.25	40.46	20.05	76.9 ± 13.1	0.77 ± 0.06	17.4 ± 7.5	1.05 ± 0.24	18.12
LEME	8.61	38.61	23.36	56.9 ± 2.3	0.72 ± 0.05	28.8 ± 3.3	0.83 ± 0.05	21.68
SHEE	10.00	39.89	60.55	40.1 ± 6.5	1.50 ± 0.32	−25.1 ± 12.6	0.79 ± 0.17	38.49
YAF	13.87	45.25	41.99	−156.6 ± 5.2	0.95 ± 0.07	99.3 ± 4.9	1.26 ± 0.07	36.79
YAYE	11.86	38.00	15.64	−109.1 ± 6.1	0.70 ± 0.08	20.6 ± 4.4	0.69 ± 0.06	11.57

the fast directions are oriented in similar or orthogonal directions. To investigate this, we plot a histogram of the strength of the lower layer and the strength from the best fitting one layer inversions (Figure 5). The strength of the lower layer/one-layer inversions is stronger beneath the MER than the Afar Depression.

8. Discussion

Previous authors have suggested many mechanisms which may cause anisotropy beneath Ethiopia, ranging from preserved structure in the lithosphere [*Gashawbeza et al.*, 2004; *Kendall et al.*, 2006], oriented melt pockets [*Gao et al.*, 1997; *Ayele et al.*, 2004; *Kendall et al.*, 2005; *Bastow et al.*, 2010; *Hammond et al.*, 2010] and flow in the mantle [*Gao et al.*, 1997; *Ayele et al.*, 2004; *Kendall et al.*, 2005; *Montagner et al.*, 2007; *Bastow et al.*, 2010; *Gao et al.*, 2010]. Our new results allow us to place constraints on the importance of these mechanisms.
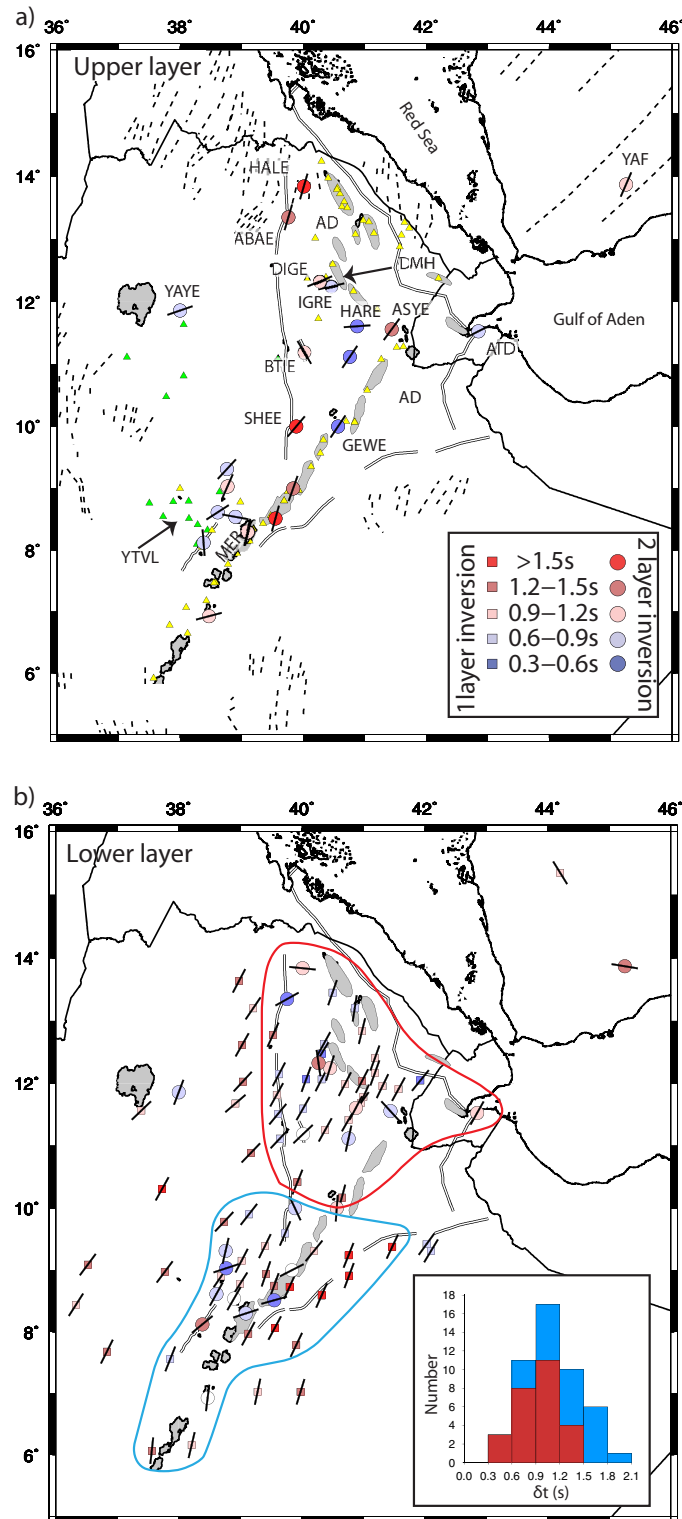
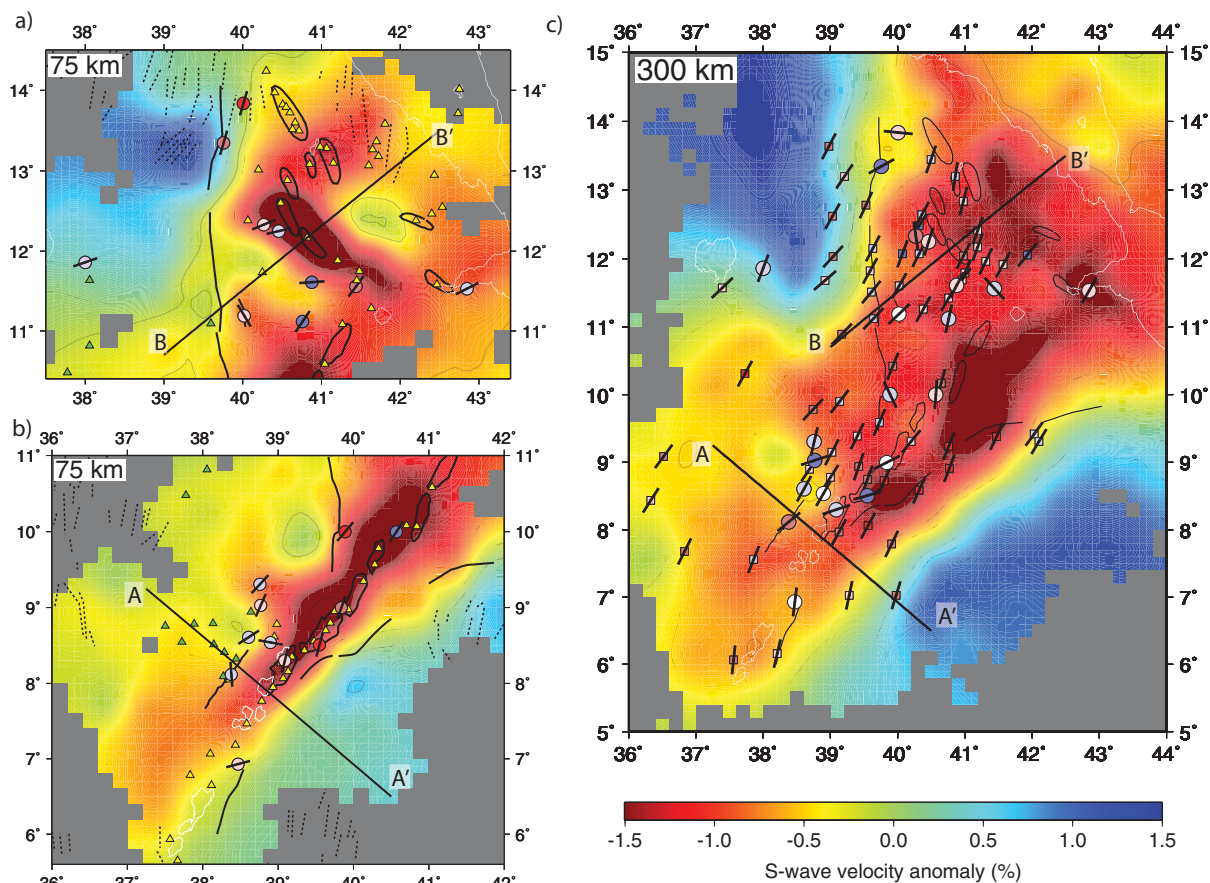### 8.1. Upper Layer
8.1.1. Ethiopian Plateau and Yemen
Our results show two examples where upper layer anisotropy seems to align with pre-existing structures beneath the western Ethiopian plateau (YAYE) and Yemen (YAF) (Figure 5). Beneath these regions thicker crust [*Hammond et al.*, 2011; *Ahmed et al.*, 2013], thicker lithosphere [*Rychert et al.*, 2012], faster mantle seismic velocities [*Hammond et al.*, 2013] (Figure 6), and relatively little active volcanism is present suggesting that fossil fabric is frozen into the Pre-Cambrian lithosphere as suggested by [*Gashawbeza et al.*, 2004; *Kendall et al.*, 2006]. Unfortunately, a lack of stations in Western Ethiopia or Yemen means this cannot be constrained fully.

8.1.2. Main Ethiopian Rift
An upper layer of anisotropy is present beneath many stations in the MER. This layer is likely due to melt in the top 90 km of the crust/mantle [*Kendall et al.*, 2005; *Bastow et al.*, 2010; *Hammond et al.*, 2010]. A strong indicator that melt is playing a role comes from the correspondence of east-west oriented upper layer fast directions which align with the east-west trending YTVL volcanic chain (Figure 5). This coincides with east-west oriented lower crustal and mantle low seismic velocities [*Daly et al.*, 2008; *Bastow et al.*, 2008; *Keranen et al.*, 2009; *Kim et al.*, 2012; *Hammond et al.*, 2013] (Figure 6), off-axis volcanism [*Abebe et al.*, 1998], and lower crustal seismicity interpreted as magma injection into the lower crust [*Keir et al.*, 2009].

Figure 5. Map showing the well constrained two-layer inversion results for (a) the upper layer and (b) lower layer. Colored circles show the δt and the bars are aligned parallel to the fast directions for all two-layer inversions which pass the tests outlined in the text. Shaded squares show the one-layer inversion results. Dashed black lines show structural trend lines in Ethiopia and Eritrea [after *Berhe*, 1990] and dotted lines show the location of major geologic terranes and boundaries in Yemen [after *Windley et al.*, 1996]. The inset in the lower plot shows the delay times for one-layer inversion results for the MER (blue) and Afar (red) corresponding to the stations enclosed by the blue and red regions, respectively. Note the larger delay times for the MER stations. AD: Afar Depression, DMH: Dabbahu-Manda-Hararo magmatic segment, MER: Main Ethiopian Rift, YTVL: Yerer-Tullu Wellel volconotectonic lineament. All other codes relate to seismic stations discussed in the text.

Figure 6. Comparison of the two-layer inversions and mantle S-wave seismic tomography. Tomography at 75 km depth beneath (a) Afar and (b) MER compared with the upper layer of anisotropy. (c) Tomography at 300 km depth compared with the lower layer of anisotropy. See Figure 5 for description of the two-layer inversion results. The gray-shaded regions show areas with <10 rays in the seismic tomography, see *Hammond et al.* [2013] for more details of the tomography.

The fact that the one-layer inversion results have a larger strength/delay time in the MER than in the Afar Depression suggests that an upper layer oriented in a similar direction to the lower layer exists beneath the MER. It is possible that the lower layer is stronger beneath the MER than Afar, but the strong evidence for low velocity zones in the top 90 km beneath the MER [*Benoit et al.*, 2006; *Bastow et al.*, 2008; *Hammond et al.*, 2013] with a clear anisotropic signature [*Kendall et al.*, 2005; *Bastow et al.*, 2010; *Hammond et al.*, 2010] suggests that an upper layer is playing a role.

8.1.3. Afar Depression
Beneath the Afar Depression there exist clear signs of an upper layer of anisotropy beneath some stations, particularly those close to the large border faults (HALE, ABAE, BTIE, and SHEE) separating the plateau from the depression and close to Quaternary-recent volcanic segments (ATD and GEWE) (Figure 5). However, large parts of the Afar Depression show best fit one-layer inversions matching the northeast-southwest regional fast directions, but with a lower strength than the MER to the south. These suggest that beneath large parts of Afar little upper layer anisotropy exists. Additionally, extra constraints on the anisotropy and velocity structure beneath the Afar Depression can be taken from surface waves [*Knox et al.*, 1998; *Sicilia et al.*, 2008; *Guidarelli et al.*, 2011] and body-wave studies [*Makris and Ginzburg*, 1987; *Keir et al.*, 2011; *Rychert et al.*, 2012; *Stork et al.*, 2013; *Hammond et al.*, 2013; *Hammond*, 2014]. Thus, to build a model which explains these Afar data, we must explain the following:

1. Regions of significant shear-wave splitting in the upper layer close to the rift margins and rift axis.

2. Very weak shear-wave splitting in the upper layer away from the rift margins and rift axis.

3. $V_{SH} < V_{SV}$ in the top 100 km beneath the Afar Depression [*Sicilia et al.*, 2008].

4. $V_{SH} > V_{SV}$ below 100 km beneath the Afar Depression [*Sicilia et al.*, 2008].

5. Strong anisotropy in the crust close to magmatic segments [*Keir et al.*, 2011; *Hammond*, 2014].

6. Strong low velocities beneath the rift axis, likely associated with melt in the top 100 km [*Makris and Ginzburg*, 1987; *Knox et al.*, 1998; *Guidarelli et al.*, 2011; *Rychert et al.*, 2012; *Stork et al.*, 2013; *Hammond et al.*, 2013] (Figure 6).

Four stations close to the western margin (HALE, ABAE, BTIE, and SHEE) show north-south orientations (Figure 5). It has been suggested that close to strong gradients in lithospheric thickness, high strains are developed and melt will be preferentially aligned [*Holtzman and Kendall*, 2010]. Afar has been shown to have little to no mantle lithosphere present compared to 75 km thick lithosphere beneath the plateau [*Rychert et al.*, 2012], and very sharp gradients in crustal thickness [*Hammond et al.*, 2011] and seismic velocity structure [*Hammond et al.*, 2013] (Figure 6) are present at this margin (Figure 7). Also, these regions of clear two-layer anisotropy are in regions where crustal V_P/V_S is highest [*Hammond et al.*, 2011], and where some of the highest crustal shear-wave splitting results are observed, again with a north-south fast direction [*Keir et al.*, 2011] (Figure 7). It seems likely that preferential alignment of melt is the dominant mechanism of anisotropy along the rift margin. This mechanism predicts that Rayleigh waves will travel at a faster velocity than Love waves ($V_{SH} < V_{SV}$). This model can explain points 1, 3, 4, and 6 above.

Geophysical imaging work in the Afar Depression has shown that the crust and mantle close to magmatic segments contain significant amounts of partial melt giving rise to anisotropic V_P/V_S [*Hammond*, 2014], low seismic velocities [*Makris and Ginzburg*, 1987; *Knox et al.*, 1998; *Guidarelli et al.*, 2011; *Hammond et al.*, 2011, 2013; *Stork et al.*, 2013], and high conductivities [*Desissa et al.*, 2013]. Much of this melt is suggested to be in the top 90 km [*Rooney et al.*, 2005; *Hammond et al.*, 2010; *Rychert et al.*, 2012; *Ferguson et al.*, 2013]. Stations close to rift axis, expressed by the presence of Quaternary-recent volcanics, show fast directions which mimic the orientation of the magmatic segments (ATD and GEWE) (Figure 5). Unfortunately, the only other segment where we have stations, the Dabbahu-Manda-Hararo (DMH) segment, does not have enough data for us to constrain two layers of anisotropy. However, it does show anomalous fast directions, with a northwest-southeast orientation, mimicking the orientation of the magmatic segment (Figure 2), and similar to the orientation seen from splitting in crustal earthquakes [*Keir et al.*, 2011]. Three stations close to DMH (DIGE, IGRE, and HARE) show more east-west fast directions in the upper layer. *Hammond* [2014] show that this mimics the orientation of anisotropy in the crust. Much of the melt is stored in the lower crust in the form of sills which gives little shear-wave splitting, but *Hammond* [2014] show that some melt is present in vertical inclusions preferentially oriented toward the volcanic segment, likely linked with the magmatic plumbing system beneath DMH. *Hammond* [2014] estimate up to 10% anisotropy in the crust close to DMH. Assuming a mantle velocity of 3.6 km s^{-1} [*Hammond et al.*, 2011], this would equate to an upper layer thickness of 39, 27, and 21 km for station DIGE, IGRE, and HARE (Figure 1). Thus, we suggest that beneath the magmatic segments a significant anisotropy from oriented melt exists mainly in the crust and uppermost mantle and the orientations are related to the crustal strain field [*Keir et al.*, 2011; *Hammond*, 2014]. Interestingly, for the stations close to the border faults a thicker upper layer (ABAE = 45 km, HALE = 81 km, BTIE = 34 km, and SHEE = 54 km) is required to explain the anisotropy (assuming 10% anisotropy). This supports the idea that at locations with sharp changes in lithospheric topography strain-derived segregation of melt in the mantle can align melt generating the anisotropy (Figure 7).

Beneath many stations in Afar, including stations above focused low velocities seen in the mantle tomography (Figure 6) little to no anisotropy in the upper layer is observed. In regions where little lithospheric topography is observed, *Holtzman and Kendall* [2010] show that anisotropy is considerably lower and that horizontal melt bands are likely to form. Shear-waves passing vertically through these melt bands will produce little shear-wave splitting. This seems to fit point 2 above, yet this model predicts $V_{SH} > V_{SV}$ through this region, the opposite of what is predicted from surface wave studies [*Sicilia et al.*, 2008]. The results from *Sicilia et al.* [2008] are based on regional data, so it is possible that melt at the steeply dipping lithospheric topography dominate the signal. However, another observation from seismic tomography is that focused
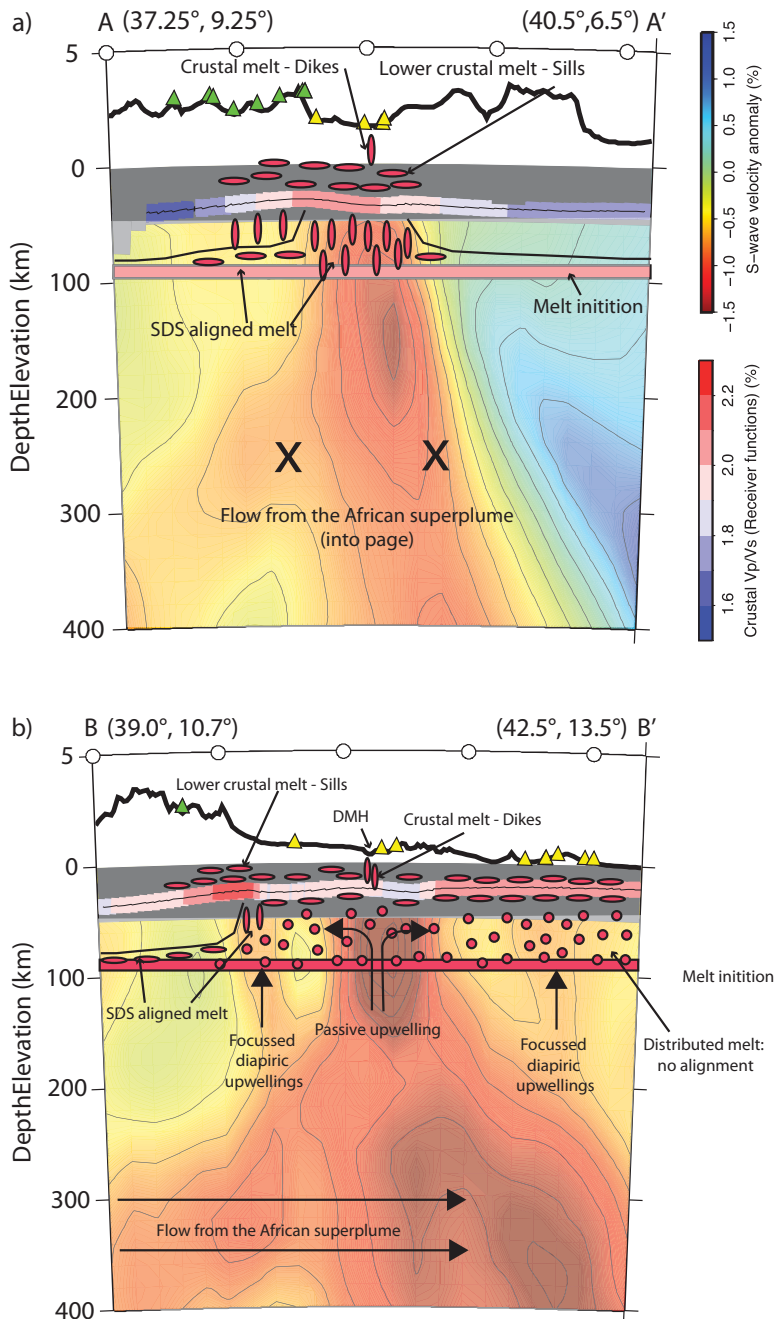
Figure 7. Annotated cross sections through (a) the MER and (b) Afar of the S-wave tomography showing the preferred models. See Figure 6 for the location of the cross sections. Also shown is topography (thick black line), crustal thickness, and bulk crustal V_P/V_S (multicolored line) [*Hammond et al.*, 2011]. The thin black line shows interpreted lithospheric thickness [after *Rychert et al.*, 2012]. Red ellipses show aligned melt and red circles show melt with little alignment. The pink band shows the region of melt initiation [*Hammond et al.*, 2010; *Rychert et al.*, 2012; *Ferguson et al.*, 2013]. Triangles show Holocene (yellow) and older (green) volcanoes.

diapiric upwellings exist in the uppermost mantle beneath Afar and passive upwelling seems to dominate beneath the rift axis [*Rychert et al.*, 2012; *Hammond et al.*, 2013]. This implies that the dominant flow mechanism in the uppermost mantle is near vertical. *Rychert et al.* [2012] suggest that little to no lithosphere is left beneath the Afar Depression, a result supported by geochemical observations in the northern Red Sea, which suggest that the lower crust and mantle lithosphere were replaced by upwelling asthenosphere before the Nubian and Arabian plates separated [*Ligi et al.*, 2012]. This implies that the considerable amount of melt in the mantle beneath Afar migrates up toward the surface and cannot form significant alignment

until it meets the crust-mantle interface. In this case, little melt anisotropy would be observed as no preferential alignment exists. Rather any anisotropy would be due to the vertical alignment of olivine crystals from vertical flow. This would cause no shear-wave splitting and ($V_{SH} < V_{SV}$), explaining points 2 and 4 above.

8.2. Mantle Flow: Lower Layer

A lower layer of anisotropy exists beneath all of Ethiopia with a consistent northeast-southwest orientation. Alignment of olivine due to flow in the mantle can generate anisotropy, yet the absence of any radial flow means a localized upwelling is unlikely. Rather, flow from the African superplume is the most likely cause, a result supported by recent thermochemical convection models [*Forte et al.*, 2010; *Faccenna et al.*, 2013]. This would induce radial anisotropy of $V_{SH} > V_{SV}$ in surface waves, explaining point 5 above. There are two locations where more north-south orientations are observed (Figure 5). These are located close to focused strong low velocities seen in mantle tomography results (Figure 6), interpreted as focused diapiric upwellings from the uppermost mantle [*Hammond et al.*, 2013]. This suggests that mantle flow may be affected in the vicinity of these small mantle upwellings. Beneath Yemen, the deeper layer of anisotropy has an east-west orientation (Figure 5), showing that the mantle flow beneath Yemen may deviate due to the presence of thicker lithosphere.

9. Conclusions

The extensive focus of seismic research in Ethiopia over the last two decades, including new deployments in the Afar Depression means that we have access to exceptional data sets across the region. These allow us to use a newly developed shear-wave splitting inversion technique [*Wookey*, 2012] which has clearly shown that two layers of anisotropy exist across much of Ethiopia. We show:

1. The MER is underlain by an upper layer, likely related to oriented melt pockets, including melt aligned oblique to the rift following the Yerer-Tullu Wellel volconotectonic lineament [*Kendall et al.*, 2005; *Bastow et al.*, 2010; *Hammond et al.*, 2010].

2. The shallow mantle beneath the Afar Depression shows evidence for aligned melt close to regions of sharp lithospheric topography [*Kendall et al.*, 2005; *Hammond et al.*, 2010; *Holtzman and Kendall*, 2010].

3. A significant upper layer of anisotropy is present close to the DMH volcanic segment which can be explained by melt alignment in the crust [*Keir et al.*, 2011; *Hammond*, 2014].

4. Away from the regions of steep LAB topography, little uppermost mantle anisotropy is observed suggesting that melt retains little preferential orientation due to the lack of mantle lithosphere and that the vertical alignment of olivine crystals dominates the anisotropic signature [*Gao et al.*, 2010].

5. The plateau regions show anisotropy consistent with fossil anisotropy frozen into the lithosphere [*Gashawbeza et al.*, 2004; *Kendall et al.*, 2006], but more data are required to constrain this.

6. A lower layer of anisotropy is evident across all of Ethiopia, and is oriented predominantly northeast-southwest. We suggest that this is linked to flow from the African superplume [*Ebinger and Sleep*, 1998; *Sleep et al.*, 2002; *Forte et al.*, 2010; *Gao et al.*, 2010; *Hansen et al.*, 2012; *Faccenna et al.*, 2013]. There is no evidence for radial flow expected for a localized upwelling from the deeper mantle.

7. The only deviations from the northeast-southwest flow in the lower layer beneath Ethiopia exist close to the locations of suspected uppermost mantle diapiric upwellings [*Hammond et al.*, 2013], suggesting these locally modify the northeast-southwest flow.

8. One station in Yemen shows signs of a more east-west orientation in the lower layer, suggesting that the lithosphere beneath Yemen may be deflecting flow to a more Gulf of Aden trend.

This study shows that melt must play an important role in late stage continental breakup, but the mechanism by which it is extracted from the mantle varies according to the stage of rifting. In the earlier stages of breakup, melt is segregated at the rift margins, as observed in the narrow MER. As rifting develops and the rift axis moves away from the margins, melt retains little preferential orientation and is extracted from the mantle by buoyancy forces alone. Evidence of this in Afar shows that, even though vestiges of continental

material remain present in the crust beneath Afar [*Makris and Ginzburg*, 1987; *Hammond et al.*, 2011], the mantle beneath this region behaves much like a slow-spreading mid-ocean ridge.

References

Abebe, T., F. Mazzarini, F. Innocenti, and P. Manetti (1998), The Yerer-Tullu Wellel volcanotectonic lineament: A transtensional structure in central Ethiopia and the associated magmatic activity, *J. Afr. Earth Sci.*, *26*(1), 135–150.

Ahmed, A., C. Tiberi, S. Leroy, G. W. Stuart, D. Keir, J. Sholan, K. Khanbari, I. Al-Ganad, and C. Basuyau (2013), Crustal structure of the rifted volcanic margins and uplifted plateau of Western Yemen from receiver function analysis, *Geophys. J. Int.*, *193*(3), 1673–1690.

Ayele, A., G. Stuart, and J. Kendall (2004), Insights into rifting from shear wave splitting and receiver functions: An example from Ethiopia, *Geophys. J. Int.*, *157*(1), 354–362.

Babuska, V., and M. Cara (1991), *Seismic Anisotropy in the Earth*, 217 pp., Kluwer Acad., Norwell, Mass.

Bagley, B., and A. A. Nyblade (2013), Seismic anisotropy in eastern Africa, mantle flow, and the African superplume, *Geophys. Res. Lett.*, *40*, 1500–1505, doi:10.1002/grl.50315.

Barruol, G., and W. Ben Ismail (2001), Upper mantle anisotropy beneath the African IRIS and GEOSCOPE stations, *Geophys. J. Int.*, *146*, 549–561.

Barruol, G., and R. Hoffmann (1999), Upper mantle anisotropy beneath the GEOSCOPE stations, *J. Geophys. Res.*, *104*(B5), 10,757–10,773.

Bastow, I. D., A. A. Nyblade, G. W. Stuart, T. O. Rooney, and M. H. Benoit (2008), Upper mantle seismic structure beneath the Ethiopian hot spot: Rifting at the edge of the African low-velocity anomaly, *Geochem. Geophys. Geosyst.*, *9*, Q12022, doi:10.1029/2008GC002107.

Bastow, I. D., S. Pilidou, J. Kendall, and G. Stuart (2010), Melt-induced seismic anisotropy and magma assisted rifting in Ethiopia: Evidence from surface waves, *Geochem. Geophys. Geosyst.*, *11*, Q0AB05, doi:10.1029/2010GC003036.

Belachew, M., C. J. Ebinger, D. Cote, D. Keir, J. Rowland, J. O. S. Hammond, and A. Ayele (2011), Comparison of dike intrusions in an incipient seafloor spreading segment in Afar, Ethiopia: Seismicity perspectives, *J. Geophys. Res.*, *116*, B06405, doi:10.1029/2010JB007908.

Benoit, M. H., A. A. Nyblade, and J. C. VanDecar (2006), Upper mantle P-wave speed variations beneath Ethiopia and the origin of the Afar hotspot, *Geology*, *34*(5), 329–332.

Berhe, S. M. (1990), Ophiolites in Northeast and East Africa: Implications for Proterozoic crustal growth, *J. Geol. Soc. London*, *147*(1), 41–57.

Blackman, D. K., and J. Kendall (1997), Sensitivity of teleseismic body waves to mineral texture and melt in the mantle beneath a mid-ocean ridge, *Philos. Trans. R. Soc. London A*, *355*, 217–231.

Blackman, J. A., D. K. Orcutt, D. W. Forsyth, and J. Kendall (1993), Seismic anisotropy in the mantle beneath an oceanic spreading center, *Nature*, *366*, 675–677.

Brisbourne, A. (2012), How to store and share geophysical data, *Astron. Geophys.*, *53*(4), 19–20.

Buck, W. R. (2004), Consequences of asthenospheric variability on continental rifting, in *Rheology and Deformation of the Lithosphere at Continental Margins*, edited by G. D. Karner et al., pp. 1–30, Columbia Univ. Press, New York.

Chang, S. J., and S. Van der Lee (2011), Mantle plumes and associated flow beneath Arabia and East Africa, *Earth Planet. Sci. Lett.*, *302*, 448–454, doi:10.1016/j.epsl.2010.12.050.

Cornwell, D. G., P. K. H. Magurie, R. W. England, and G. W. Stuart (2010), Imaging detailed crustal structure and magmatic intrusion across the Ethiopian rift using a dense linear broadband array, *Geochem. Geophys. Geosyst.*, *11*, Q0AB03, doi:10.1029/2009GC002637.

Daly, E., D. Keir, C. J. Ebinger, G. W. Stuart, I. D. Bastow, and A. Ayele (2008), Crustal tomographic imaging of a transitional continental rift: The Ethiopian rift, *Geophys. J. Int.*, *172*, 1033–1048.

Desissa, M., N. E. Johnson, K. A. Whaler, S. Hautot, S. Fisseha, and G. Dawes (2013), Mantle magma reservoir imaged magnetotellurically beneath the proto-mid-ocean ridge in Afar, Ethiopia, *Nat. Geosci.*, *6*, 861–865.

Druken, K., C. Kincaid, and R. Griffiths (2013), Directions of seismic anisotropy in laboratory models of mantle plumes, *Geophys. Res. Lett.*, *40*, 3544–3549, doi:10.1002/grl.50671.

Ebinger, C. J., and M. Casey (2001), Continental breakup in magmatic provinces: An Ethiopian example, *Geology*, *29*, 527–530.

Ebinger, C. J., and N. H. Sleep (1998), Cenozoic magmatism throughout east Africa resulting from impact of a single plume, *Nature*, *395*, 788–791.

Ebinger, C. J., D. Keir, A. Ayele, E. Calais, T. J. Wright, M. Belachew, J. O. S. Hammond, E. Campbell, and W. R. Buck (2008), Capturing magma intrusion and faulting processes during continental rupture: Seismicity of the Dabbahu (Afar) rift, *Geophys. J. Int.*, *174*, 1138–1152.

Faccenna, C., T. W. Becker, L. Jolivet, and M. Keskin (2013), Mantle convection in the Middle East: Reconciling Afar upwelling, Arabia indentation and Aegean trench rollback, *Earth Planet. Sci. Lett.*, *375*, 254–269.

Ferguson, D., J. Maclennan, I. Bastow, D. Pyle, S. Jones, D. Keir, J. Blundy, T. Plank, and G. Yirgu (2013), Melting during late-stage rifting in Afar is hot and deep, *Nature*, *499*, 70–73.

Forte, A., S. Quéré, R. Moucha, N. Simmons, S. Grand, J. Mitrovica, and D. Rowley (2010), Joint seismic-geodynamic-mineral physical model-ling of African geodynamics: A reconciliation of deep-mantle convection with surface geophysical constraints, *Earth Planet. Sci. Lett.*, *295*, 329–341.

Gao, S., P. M. Davies, H. Liu, P. D. Slack, A. W. Rigor, Y. A. Zorin, V. V. Mordvinova, V. M. Kozhevnikov, and N. A. Logatchev (1997), SKS split-ting beneath continental rift zones, *J. Geophys. Res.*, *102*(B10), 22,781–22,797, doi:10.1029/97JB01858.

Gao, S., K. Liu, and M. Abdelsalam (2010), Seismic anisotropy beneath the Afar Depression and adjacent areas: Implications for mantle flow, *J. Geophys. Res.*, *115*, B12330, doi:10.1029/2009JB007141.

Gashawbeza, E. M., S. L. Klemperer, A. A. Nyblade, K. T. Walker, and K. M. Keranen (2004), Shear-wave splitting in Ethiopia: Precambrian mantle anisotropy locally modified by Neogene rifting, *Geophys. Res. Lett.*, *31*, L18602, doi:10.1029/2004GL020471.

Guidarelli, M., G. Stuart, J. O. S. Hammond, J. Kendall, A. Ayele, and M. Belachew (2011), Surface wave tomography across Afar, Ethiopia: Crustal structure at a rift triple-junction zone, *Geophys. Res. Lett.*, *38*, L24313, doi:10.1029/2011GL046840.

Hammond, J. O. S. (2014), Constraining melt storage geometries beneath the Afar Depression, Ethiopia from teleseismic receiver functions: The anisotropic H-κ stacking technique, *Geochem. Geophys. Geosyst.*, doi:10.1002/2013GC005186, in press.

Hammond, J. O. S., J. Kendall, D. Angus, and J. Wookey (2010), Interpreting spatial variations in anisotropy: Insights into the Main Ethiopian Rift from SKS waveform modelling, *Geophys. J. Int.*, *181*, 1701–1712.

Hammond, J. O. S., J. Kendall, G. W. Stuart, D. Keir, C. J. Ebinger, A. Ayele, and M. Belachew (2011), The nature of the crust beneath the Afar triple junction: Evidence from receiver functions, *Geochem. Geophys. Geosyst.*, *12*, Q12004, doi:10.1029/2011GC003738.

Hammond, J. O. S., et al. (2013), Mantle upwelling and initiation of rift segmentation beneath the Afar Depression, *Geology*, *41*, 635–638.

Hansen, S. E., A. A. Nyblade, and M. H. Benoit (2012), Mantle structure beneath Africa and Arabia from adaptively parameterized P-wave tomography: Implications for the origin of Cenozoic Afro-Arabian tectonism, *Earth Planet. Sci. Lett.*, *319–320*, 23–34, doi:10.1016/j.epsl.2011.12.023.

Harmon, N., D. Forsyth, K. Fischer, and S. Webb (2004), Variations in shear-wave splitting in young Pacific seafloor, *Geophys. Res. Lett.*, *31*, L15609, doi:10.1029/2004GL020495.

Holtzman, B. K., and J. Kendall (2010), Organized melt, seismic anisotropy and plate boundary lubrication, *Geochem. Geophys. Geosyst.*, *11*, Q0AB06, doi:10.1029/2010GC003296.

Keir, D., J. Kendall, C. J. Ebinger, and G. W. Stuart (2005), Variations in late syn-rift melt alignment inferred from shear-wave splitting in crustal earthquakes beneath the Ethiopian rift, *Geophys. Res. Lett.*, *32*, L23308, doi:10.1029/2005GL024150.

Keir, D., et al. (2009), Evidence for focused magmatic accretion at segment centers from lateral dike injections captured beneath the Red Sea rift in Afar, *Geology*, *37*, 59–62.

Keir, D., M. Belachew, C. J. Ebinger, J. Kendall, J. O. S. Hammond, G. W. Stuart, and A. Ayele (2011), Mapping the evolving strain field in the Afar Triple Junction using crustal anisotropy, *Nat. Comm.*, *2*, 285, doi:10.1038/ncomms1287.

Kendall, J. (1994), Teleseismic arrivals at a mid-ocean ridge: Effects of mantle melt and anisotropy, *Geophys. Res. Lett*, *21*(4), 301–304.

Kendall, J. (2000), Seismic anisotropy in the boundary layers of the mantle, in *Earth's Deep Interior: Mineral Physics and Tomography From the Atomic to the Global Scale, Geophys. Monogr. Ser.*, vol. 117, edited by S. Karato, et al., pp. 133–159, American Geophysical Union, Washington DC.

Kendall, J., G. W. Stuart, C. J. Ebinger, I. D. Bastow, and D. Keir (2005), Magma-assisted rifting in Ethiopia, *Nature*, *433*(7022), 146–148.

Kendall, J., S. Pilidou, D. Keir, I. D. Bastow, G. W. Stuart, and A. Ayele (2006), Mantle upwellings, melt migration and the rifting of Africa: Insights from seismic anisotropy, in The Afar Volcanic Province Within the East African Rift System, vol. 259, edited by G. Yirgu et al., pp. 55–72, Geol. Soc. Spec. Publ., London.

Keranen, K. M., S. L. Klemperer, J. Julia, J. F. Lawrence, and A. A. Nyblade (2009), Low lower crustal velocity across Ethiopia: Is the Main Ethiopian Rift a narrow rift in a hot craton?, *Geochem. Geophys. Geosyst.*, *10*, Q0AB01, doi:10.1029/2008GC002293.

Kim, S., A. A. Nyblade, J. Rhie, C. E. Baag, and T. S. Kang (2012), Crustal S-wave velocity structure of the Main Ethiopian Rift from ambient noise tomography, *Geophys. J. Int.*, *191*, 865–878.

Knox, R. P., A. A. Nyblade, and C. A. Langston (1998), Upper mantle S velocities beneath Afar and western Saudi Arabia from Rayleigh wave dispersion, *Geophys. Res. Lett.*, *25*, 4233–4236.

Ligi, M., E. Bonatti, G. Bortoluzzi, A. Cipriani, L. Cocchi, F. C. Tontini, E. Carminati, L. Ottolini, and A. Schettino (2012), Birth of an ocean in the Red Sea: Initial pangs, *Geochem. Geophys. Geosyst.*, *13*, Q08009, doi:10.1029/2012GC004155.

Maguire, P. K. H., et al. (2003), Geophysical project in Ethiopia studies continental breakup, *Eos Trans. AGU*, *84*(35), 337–343, doi:10.1029/2003EO350002.

Makris, J., and A. Ginzburg (1987), The Afar depression: Transition between continental rifting and sea-floor spreading, *Tectonophysics*, *141*, 199–214.

Montagner, J. (1998), Where can seismic anisotropy be detected in the Earth's mantle? In boundary layers., *Pure Appl. Geophys.*, *151*, 223–256.

Montagner, J., et al. (2007), Mantle upwellings and convective instabilities revealed by seismic tomography and helium isotope geochemistry beneath eastern Africa, *Geophys. Res. Lett*, *34*, L21303, doi:10.1029/2007GL031098.

Nyblade, A. A., and C. A. Langston (2002), Broadband seismic experiments probe the East African Rift, *Eos Trans AGU*, *83*(405), 407–408.

Obrebski, M., S. Kiselev, L. Vinnik, and J. Montagner (2010), Anisotropic stratification beneath Africa from joint inversion of SKS and P receiver functions, *J. Geophys. Res.*, *115*, B09313, doi:10.1029/2009JB006923.

Restivo, A., and G. Helffrich (1999), Teleseismic shear wave splitting measurements in noisy environments, *Geophys. J. Int.*, *137*, 821–830.

Rogers, N. W. (2006), Basaltic magmatism and the geodynamics of the East African Rift System, in The Afar Volcanic Province Within the East African Rift System, vol. 259, edited by G. Yirgu et al., pp. 77–94, Geol. Soc. Spec. Publ., London.

Rooney, T., T. Furman, G. Yirgu, and D. Ayalew (2005), Structure of the Ethiopian lithosphere: Xenolith evidence in the Main Ethiopian Rift, *Geochim. Cosmochim. Acta*, *69*(15), 3889–3910.

Rümpker, G., and P. G. Silver (2000), Calculating splitting parameters for plume-type anisotropic structures of the upper mantle, *Geophys. J. Int.*, *143*, 507–520.

Rychert, C. A., J. O. S. Hammond, N. Harmon, J. Kendall, D. Keir, C. Ebinger, I. Bastow, A. Ayele, M. Belachew, and G. Stuart (2012), Volcanism in the Afar rift sustained by decompression melting with minimal plume influence, *Nat. Geosci.*, *5*, 406–409, doi:10.1038/ngeo1455.

Savage, M. K. (1999), Seismic anisotropy and mantle deformation: What have we learned from shear wave splitting?, *Rev. Geophys.*, *37*(1), 65–106.

Sebai, A., E. Stutzmann, J. Montagner, D. Sicilia, and E. Beucler (2006), Anisotropic structure of the African upper mantle from Rayleigh and Love wave tomography, *Phys. Earth Planet. Inter.*, *155*(1–2), 48–62.

Sicilia, D., et al. (2008), Upper mantle structure of shear-waves velocities and stratification of anisotropy in the afar hotspot region, *Tectonophysics*, *462*(1–4), 164–177.

Silver, P. G. (1996), Seismic anisotropy beneath the continents: Probing the depths of geology, *Annu. Rev. Earth Planet. Sci*, *24*, 385–432.

Silver, P. G., and W. W. J. Chan (1991), Shear-wave splitting and subcontinental mantle deformation, *J. Geophys. Res.*, *96*, 16,429–16,454.

Silver, P. G., and M. K. Savage (1994), The interpretation of shear wave splitting parameters in the presence of two anisotropic layers, *Geophys. J. Int.*, *119*, 949–963.

Slack, P. D., P. M. Davis, and Kenya Rift International Seismic Project (KRISP) Teleseismic Working Group (1994), Attenuation and velocity of P-waves in the mantle beneath the East African Rift, Kenya, *Tectonophysics*, *236*(1), 331–358.

Sleep, N. H., C. J. Ebinger, and J. Kendall (2002), Deflection of mantle plume material by cratonic keels, in Early Earth, edited by C. M. Fowler et al., pp. 135–150, Geol. Soc. Spec. Publ., London.

Stork, A., G. W. Stuart, C. M. Henderson, D. Keir, and J. O. S. Hammond (2013), Uppermost mantle (Pn) velocity model for the Afar region, Ethiopia: An insight into rifting processes, *Geophys. J. Int.*, *193*, 321–328.

Teanby, N. A., J. Kendall, and M. Van der Baan (2004), Automation of shear-wave splitting measurements using cluster analysis, *Bull. Seismol. Soc. Am.*, *94*(2), 453–463.

Vauchez, A., A. Tommasi, G. Barruol, and J. Maumus (2000), Upper mantle deformation and seismic anisotropy in continental rifts, *Phys. Chem. Earth*, *25*, 111–117.

Windley, B. F., M. J. Whitehouse, and M. A. O. Ba-Bttat (1996), Early Precambrian gneiss terranes and Pan-African island arcs in Yemen: Crustal accretion of the eastern Arabian Shield, *Geology*, *24*(2), 131–134.

Wolfe, C. J., and P. G. Silver (1998), Seismic anisotropy of oceanic upper mantle: Shear wave splitting methodologies and observations, *J. Geophys. Res.*, *103*, 749–771.

Wolfe, C. J., and S. C. Solomon (1998), Shear-wave splitting and implications for mantle flow beneath the MELT region of the East Pacific Rise, *Science*, *280*, 1230–1232.

Wookey, J. (2012), Direct probabilistic inversion of shear-wave data for seismic anisotropy, *Geophys. J. Int.*, *189*, 1025–1037, doi:10.1111/j.1365-246X.2012.05405.x.

Wustefeld, A., and G. Bokelmann (2007), Null detection in shear-wave splitting measurements, *Bull. Seismol. Soc. Am*, *97*(4), 1204–1211.

Wustefeld, A., O. Al-Harrasi, J. P. Verdon, J. Wookey, and J. Kendall (2010), A strategy for automated analysis of passive microseismic data to image seismic anisotropy and fracture characteristics, *Geophysics*, *58*, 755–773.